Preclinical evaluation of potential infection-imaging probe [^{68}Ga]Ga-DOTA-K-A9 in sterile and infectious inflammation

Nielsen, Karin M; Jørgensen, Nis P; Kyneb, Majbritt H; Borghammer, Per; Meyer, Rikke L; Thomsen, Trine R; Bender, Dirk; Jensen, Svend B; Nielsen, Ole L; Alstrup, Aage K O

Published in:
Journal of Labelled Compounds and Radiopharmaceuticals

DOI (link to publication from Publisher):
10.1002/jlcr.3640

Publication date:
2018

Document Version
Accepted author manuscript, peer reviewed version

Preclinical evaluation of potential infection-imaging probe [^{68}Ga]Ga-DOTA-K-A9 in sterile and infectious inflammation

Karin M. Nielsen[a, b,c] *, Nis P. Jørgensen[d], Majbritt H. Kyneb[e], Per Borghammer[f], Rikke L. Meyer[g], Trine R. Thomsen[e, h], Dirk Bender[f], Svend B. Jensen[b,i], Ole L. Nielsen[c], Aage K. O. Alstrup[f]

[a] Department of Clinical Physiology and Nuclear Medicine, Copenhagen University Hospital, Herlev, DK-2730 Herlev, Denmark

[b] Department of Nuclear Medicine, Aalborg University Hospital, DK-9000 Aalborg, Denmark

[c] Department of Veterinary Disease Biology, Faculty of Health and Medical Sciences, University of Copenhagen, DK-1870 Copenhagen, Denmark

[d] Department of Infectious Diseases & Department of Clinical Microbiology, Institute of Clinical Medicine, Aarhus University Hospital, DK-8000 Aarhus, Denmark

[e] Biotech, Life Science, Danish Technological Institute, DK-8000 Aarhus, Denmark

[f] Department of Nuclear Medicine and PET-centre, Aarhus University Hospital, DK-8000 Aarhus, Denmark

[g] Interdisciplinary Nanoscience Center, Aarhus University, DK-8000 Aarhus, Denmark

[h] Department of Biotechnology, Aalborg University, DK-9000 Aalborg, Denmark

[i] Department of Chemistry and Biochemistry, Aalborg University, DK-9000 Aalborg, Denmark

* Corresponding author: Department of Clinical Physiology and Nuclear Medicine, Copenhagen University Hospital, Herlev, Herlev Ringvej 75, DK-2730 Herlev, Denmark. Tel: +45 38686441, email: karin.michaelsen.nielsen@regionh.dk (K. M. Nielsen)

This article has been accepted for publication and undergone full peer review but has not been through the copyediting, typesetting, pagination and proofreading process which may lead to differences between this version and the Version of Record. Please cite this article as doi: 10.1002/jlcr.3640

Abstract

The development of bacteria-specific infection radiotracers is of considerable interest to improve diagnostic accuracy and enabling therapy monitoring. The aim of this study was to determine if the previously reported radiolabelled 1,4,7,10-tetraazacyclododecane-N,N′,N″,N‴-tetraacetic acid (DOTA) conjugated peptide, [^{68}Ga]Ga-DOTA-K-A9 could detect a staphylococcal infection *in vivo*, and distinguish it from aseptic inflammation. An optimised [^{68}Ga]Ga-DOTA-K-A9 synthesis omitting the use of acetone was developed, yielding 93% ± 0.9% radiochemical purity. The *in vivo* infection binding specificity of [^{68}Ga]Ga-DOTA-K-A9 was evaluated by micro positron emission tomography/magnetic resonance imaging (μPET/MRI) of 15 mice with either subcutaneous *S. aureus* infection or turpentine induced inflammation and compared with 2-deoxy-2-[^{18}F]fluoro-D-glucose ([^{18}F]FDG). The scans showed that [^{68}Ga]Ga-DOTA-K-A9 accumulated in all the infected mice at injected doses ≥3.6 MBq. However, the tracer was not found to be selective towards infection, since the [^{68}Ga]Ga-DOTA-K-A9 also accumulated in mice with inflammation.

In a concurrent *in vitro* binding evaluation performed with a 5-Carboxytetramethylrhodamine (TAMRA) fluorescence analogue of the peptide, TAMRA-K-A9, the microscopy results suggested that TAMRA-K-A9 bound to an intracellular epitope and therefore preferentially targeted dead bacteria. Thus, the [^{68}Ga]Ga-DOTA-K-A9 uptake observed *in vivo* is presumably a combination of local hyperaemia, vascular leakiness and/or binding to an epitope present in dead bacteria.

Keywords: PET, gallium-68, [^{68}Ga]Ga-DOTA-K-A9, bacterial infection, *S. aureus*, murine models, fluorescence.

1 Introduction

Timely and accurate diagnosis of bacterial infections is essential for successful patient treatment. In addition to conventional analyses of blood, urine, or tissue biopsy, diagnosis is often made with non-invasive imaging modalities i.e. anatomical or functional.[1-3] However, with anatomical imaging techniques, such as magnetic resonance imaging (MRI) and computed tomography (CT), an infection only becomes apparent when the lesion has resulted in anatomical changes. Thus, CT and MRI are frequently applied in combination with the functional imaging technique of positron emission tomography (PET) that allows detection of early pathophysiologic changes prior to anatomical alterations. A general shortcoming of the commonly used radiotracers targeting the immune response, including 2-deoxy-2-[^{18}F]fluoro-D-glucose ([^{18}F]FDG), are their inability to distinguish between different sources of inflammation, i.e. between sterile inflammation, infection or malignancy.[4,5]

The development of bacteria-specific radiotracers for infection is therefore of considerable interest to improve diagnostic accuracy and thereby patient treatment. The field of developing bacteria-specific radiotracers, targeting unique bacterial characteristics, has been explored during the past decades;[1,3,6] among the most extensively researched tracers are the radiolabelled antibiotic ciprofloxacin and the antimicrobial peptide ubiquicidin.[7-13] Recently, the development of bacteria-specific tracers, e.g. 2-[^{18}F]-fluorodeoxysorbitol and ^{18}F-labelled maltohexaose, have exploited the differences in sugar metabolism of bacteria and human cells with promising results.[14,15] In most cases, however, it is unknown if or to what extent the developed bacteria-specific imaging probes bind to bacteria aggregated in biofilms *in vivo*.[3]

S. aureus is a major cause of soft tissue, endovascular, bone and post-surgical infections, and is often associated with abscess and biofilm formation.[16,17] We have earlier reported the identification of the dodecapeptide A9 by phage-display selection against *S. aureus* biofilm,

as well as the gallium-68 labelling, and initial biological evaluation of the 1,4,7,10-tetraazacyclododecane-N,N′,N″,N‴-tetraacetic acid (DOTA) conjugated peptide DOTA-K-A9 (FigureA) as a potentially bacteria-specific PET-tracer.[18]

The purpose of this study was to further investigate if the [^{68}Ga]Ga-DOTA-K-A9 was able to differentiate between infected and aseptic inflamed tissues using µPET/MRI and compare it to [^{18}F]FDG in murine subcutaneous (SC) infection and inflammation models. A parallel *in vitro* binding evaluation of the 5-Carboxytetramethylrhodamine (TAMRA) fluorescence analogue, TAMRA-K-A9 (FigureB), was performed with different viable and dead bacterial cultures to further characterise the bacterial binding of the A9 peptide.

2 Experimental

2.1 *Materials*

All chemicals were of analytical grade or better and used without further purification. The main suppliers were Sigma-Aldrich (Brøndby, Denmark) and Merck (Darmstadt, Germany). Aqueous solutions for high performance liquid chromatography (HPLC) analysis were prepared with deionised distilled water (Milli-Q water system; Millipore, Aarhus, Denmark). In all other aqueous solutions water for injection (Danish Capital Region Pharmacy) was applied. The DOTA-K-A9 peptide for gallium-68 labelling and the fluorescence analogue of the peptide TAMRA-K-A9 were custom synthesised by Pepscan (Lelystad, The Netherlands). The membrane-impermeable DNA-binding stain TOTO®-1 was bought from Thermo Fisher (Nærum, Denmark). [^{68}Ga]$GaCl_3$ for radiolabelling was obtained from an IGG100-50M gallium-68 generator commercially available from Eckert & Ziegler (Berlin, Germany), yielding in the range of 0.6 - 1.0 GBq.

Cationic exchange cartridges Varian SCX (50 µg, 1 ml) were from Agilent Technologies (Glostrup, Denmark). Sep-Pak (55-105 µm particles) C18-light (130 mg) cartridges were

obtained from Waters (Hedehusene, Denmark). The gallium-68 labelling was performed with reused, commercially available cassettes, which were washed and applied with new cartridges.

Radiosyntheses were done on an automated ModularLab PharmTracer synthesis module from Eckert & Ziegler (Berlin, Germany) employing a self-designed synthesis program [19]. Purity analyses of the radiolabelled compounds were performed using reversed-phase HPLC on an Ultimate 3000 system from Dionex (Hvidovre, Denmark) and thin-layer chromatography (TLC) on a PET miniGita* TLC scanner from Raytest (Straubenhardt, Germany). The acetone and ethanol content in the product was analysed by Gas Chromatography (GC) on a Clarus 480 GC from Perkin Elmer (Skovlunde, Denmark), pH-values were measured applying a PH M220 pH-meter from Radiometer Analytical (Villeurbanne, France), and the radioactivity of the products was determined by a VDC-405 dose calibrator from Veenstra Instruments (Joure, The Netherlands).

The binding selectivity of [^{68}Ga]Ga-DOTA-K-A9 was evaluated by µPET/MRI on mice using an integrated Mediso NanoScan® PET/MRI system from Mediso Medical Imaging Systems (Budapest, Hungary).

2.2 *Bacteria*

The different bacteria used in the study are listed in Table 1. The *S. aureus* isolate originating from a clinical prosthesis infection, which was used to prepare the biofilm applied in the preceding phage-display selection of the A9 peptide,[18] was also used in both the murine SC infection model and *in vitro* evaluation of TAMRA-K-A9. The bacteria were grown overnight from a single colony in tryptic soy broth (TSB) at 37 °C while being gently shaken at 200 rpm on an incubator shaker (IKA KS 4000i control, from VWR). Following overnight incubation, the bacteria suspension was density adjusted according to 600 nm absorbance

with TSB (5x 10^7 colony forming unit (CFU)/ml) for the mice inoculation. For the morphological *in vitro* evaluation, samples of dead bacteria were additionally prepared by immersing a swap in each of the fresh bacteria cultures and subsequently transferring the swaps with bacteria to tubes containing CyMol® (COPAN, Italy) and incubated for 10 min at room temperature, to kill the bacteria. Then the tubes were vortexed shortly, before the solutions (1 ml each) were transferred to new tubes.

2.3 *Radiochemistry*

2.3.1 Initial gallium-68 labelling of DOTA-K-A9

The [^{68}Ga]Ga-DOTA-K-A9 for the mice pilot infection study was prepared as previously described.[18] Briefly, approx. 1.0 GBq [^{68}Ga]$GaCl_3$ was eluted from the generator with 0.1 M HCl (10 ml) and trapped on a Strata-X-C cartridge, before it was eluted with a 0.02 M HCl/ acetone (97.6%) solution (600 µl). The [^{68}Ga]Ga-DOTA-K-A9 was synthesised by dissolving DOTA-K-A9 (66 µg, 35 nmol) in 0.1 M 2-[4-(2-hydroxyethyl)piperazin-1-yl]-ethanesulfonic acid (HEPES) aq. solution (5 ml) pH 4, adjusted with 30% HCl, added pre-purified [^{68}Ga]$GaCl_3$ (600 µl) and heated at 95 °C for 5 min. The [^{68}Ga]Ga-DOTA-K-A9 formulation (pH 3.9 - 4.1) was used without further purification, but diluted with saline to obtain an acetone content <4000 ppm in the *in vivo* injections.

2.3.2 Optimized gallium-68 labelling of DOTA-K-A9

In the optimised production of [^{68}Ga]Ga-DOTA-K-A9, which was applied in the mice infection and inflammation comparison study, approx. 0.6 GBq [^{68}Ga]$GaCl_3$ from the generator was trapped on a Varian SCX cartridge and eluted with a 5 M NaCl/ 5.5 M HCl (2.5%) solution (700 µl).[20] The following gallium-68 labelling was achieved by mixing the pre-purified [^{68}Ga]$GaCl_3$ with the precursor DOTA-K-A9 (70 µg, 37 nmol) in 0.1 M HEPES

aq. solution pH 6.5 (5 ml) and heated at 95 °C for 3.5 min. The purification of [^{68}Ga]Ga-DOTA-K-A9 was performed using a C18-light cartridge, pre-conditioned with 50% EtOH aq. solution (5 ml) and 0.1 M HEPES aq. solution pH 5.2 (5 ml). The pre-conditioning of the C18-light cartridge was performed by the automated synthesis module during the 3.5 min labelling of the peptide in the reactor. First, the 50% EtOH aq. solution (5 ml) was passed through the C18-light cartridge followed by air (10 ml); second, the cartridge was washed with the 0.1 M HEPES aq. solution (5 ml) and dried again with air (10 ml).

After the 3.5 min labelling reaction, the [^{68}Ga]Ga-DOTA-K-A9 reaction mixture was immediately transferred and trapped on the C18-light cartridge and rinsed with 0.1 M HEPES aq. solution pH 5.2 (2 ml), before it was eluted with 50% EtOH aq. solution (1 ml). The final formulation (9 ml) of the product was achieved by adding isotonic saline (8 ml). The stability of the [^{68}Ga]Ga-DOTA-K-A9 in the product formulation (pH 5.1 - 5.7) was evaluated up to 120 min employing the radio-HPLC setup described in the next section. The product formulation was further diluted prior to the biological testing in mice, to achieve an ethanol content <5 % (v/v).

2.3.3 Quality control

Decay corrected radiochemical yield, and radiochemical purity were determined using radio-TLC and radio-HPLC. The radio-TLC analysis applied silica iTLC sheets from Agilent technologies as the stationary phase, and two different mobile phases. Mobile phase I, 0.1 M sodium citrate pH 5.5 with the following retention factors (R_f): 0.12 ± 0.03 for [^{68}Ga]Ga-DOTA-K-A9 and 0.85 ± 0.07 for free gallium-68 ions binding to the citrate. Mobile phase II, 50% 1 M ammonium acetate in methanol with the corresponding R_f: 0.72 ± 0.14 for [^{68}Ga]Ga-DOTA-K-A9 and 0.02 ± 0.02 for gallium-68 colloid.

The analytical HPLC of [^{68}Ga]Ga-DOTA-K-A9 was performed using an Aeris Peptide XB-C18 column (2.6 µm, 150x4.6 mm) from Phenomenex. Here, a binary gradient system with a 1.0 ml/min flow rate employing 0.1% trifluoroacetic acid (TFA) in water (A) and 0.1% TFA in acetonitrile (B) as mobile phases was applied. The mobile phase gradient was as following: 0-10 min, linear gradient 9.5 to 15% of B; from 10-12 min, linear gradient from 15 to 70% B; 2 min at 70% B; 2 min decrease in B to 9.5%; 16-20 min at 9.5% B. The compounds were eluted: [^{68}Ga]$GaCl_3$ at 1.7 ± 0.1 min, DOTA-K-A9 at 6.6 ± 0.2 min, [^{68}Ga]Ga-DOTA-K-A9 7.1 ± 0.5 min.

2.4 *In vivo evaluation*

2.4.1 Animals

The studies in mice were performed according to the Danish Animal Experimentation Act and the European Convention for the protection of vertebrate animals used for experimental and other scientific purposes (ETS No. 123) and the European Union directive on the protection of animals used for scientific purposes (2010/63/EU). The Danish Animal Experiments Inspectorate granted the animal experiment license (2015-15-0201-00631).

In this study, C57Bl6/J mice (n = 17, adult, females, 20-22 g) were applied, with the analyses performed on each mouse shown in Table 2. The mice for the pilot infection study (n = 3) were purchased from M&B Taconic, while the mice in the main infection and inflammation comparison study came from Janvier Labs. All animals had an acclimatisation period of minimum 7 days at the experimental animal facility. They were housed with a 12 h light/dark cycle and had access to tap water *ad libitum* and pellet feed.

During the scans the animals were placed on a gantry which regulated the temperature to 37 °C and they were kept lightly anesthetised by isoflourane in an oxygene-medical air mixture

through a mask, while they were removed from anaesthesia between scans. After the last PET scan, the mice were euthanised by cervical dislocation while still anaesthetised. No blood samples were taken during the µPET/MRI experiment.

2.4.2 Murine infection and inflammation models

The mice were anaesthetised with isofluorane inhalation and pre-operative intra muscular injection of buprenorphine (Temgesic, 30 µg/ml, 100 µl). A skin area of approx. 1.5 cm^2 above right scapula was shaved and washed with 70% ethanol. After the ethanol had evaporated, either *S. aureus* in TSB suspension (5x 10^7 CFU/ml, 100 µl) or turpentine (100%, 100 µl) was injected SC. The hypodermic needle was kept *in situ* for 5 sec post-injection to prevent retrograde leakage of bacterial suspension. Animals were returned to their cages until the µPET/MRI-scan were conducted 27 ± 2 h later. Humane endpoints were defined as systemic illness, impaired mobility, treatment refractory pain or acute weight loss >15%. Post-inoculated, the mice in the comparison study had access to buprenorphine 6.0 µg/ml through the drinking water.

2.4.3 µPET/ MRI imaging

In the pilot study, three anesthetised mice with SC infection underwent a 100 min whole body dynamic PET scan immediately after intravenous injection of 3.2 ± 1.5 MBq [^{68}Ga]Ga-DOTA-K-A9, through the tail vein (200-300 µl). A 15 min T2 weighted MRI sequence was subsequently acquired for anatomical localisation. Five hours later, allowing for decay of the [^{68}Ga]Ga-DOTA-K-A9, a 100 min dynamic PET scan was performed 60 min post-injection of 11.7 ± 7.3 MBq [^{18}F]FDG (100-200 µl) followed again by a 15 min MRI scan.

A similar setup, as described above, was applied in the SC infection and inflammation comparison study, except for a reduced PET scan time from 100 to 60 min (Figure 2) and the

[^{68}Ga]Ga-DOTA-K-A9 being prepared by the optimised method (Section 2.3.2). The mice (n = 12) received an intravenous injection of 7.3 ± 2.9 MBq [^{68}Ga]Ga-DOTA-K-A9 (300 µl) and later 9.5 ± 4.3 MBq of [^{18}F]FDG (<70 µl).

Anatomical localisation was performed by T2 weighted MRI sequence (matrix size 200x192, field-of-view 80 mm, 1.0 mm slice thickness, 25 slices, slice gap 0.1 mm, TR/TE 4999/80 ms; NEX 2). All PET scans were corrected for randoms and reconstructed using a 3D-OSEM iterative reconstruction algorithm (Tera-Tomo 3D; 4 iterations, 6 subsets; voxel size 0.4x0.4x0.4 mm). No correction was made for attenuation and scatter.

The PET scans were evaluated by a nuclear physician. Sites of infection or inflammation were located on the PET images, and the anatomical location in the subcutis was verified on the MRI images. The uptake values of the four hottest voxels on five consecutive images slices were averaged. Two different reference regions were defined (>20 voxels) in the contra-lateral SC region and shoulder muscle (*musculus acromiotrapezius*), respectively. Finally, two lesion-to-background ratios were calculated by dividing the average uptake in the infection/inflammation locus by the average uptake in the reference regions.

2.4.4 Post-mortem microbiology and histopathology analyses

Abscesses from the scanned mice (Table 2) were aseptically excised *in toto* and collected individually in Precellys MK28 tubes from Bertin Technologies (Saint Quentin, France) containing ceramic beads. The tubes with abscesses were stored for 1 h at 2 °C before the addition of sterile phosphate buffered saline (PBS) (500 µl, 5 °C) and immediate transfer to a bead beater (Precellys 24 tissue homogeniser, Bertin Technologies). Homogenisation of the abscess was achieved by running a sequence of 5000 rpm in 2x 20 sec, followed by 10 min storage at 2 °C and repetition of the sequence. This yielded fully homogenised liquid abscess samples from which serial 10-fold dilutions in sterile PBS were performed in triplicates. Each

dilution (10 µl) was seeded on 5% blood agar plates from SSI Diagnostic (Hillerød, Denmark) and incubated for 24 h at 37 °C before counting CFU.

To characterise the models histologically, tissue representing the SC lesions was removed from selected mice as shown in Table 2. Tissue samples were fixed in 3.7% neutral buffered formaldehyde for several days, dehydrated, embedded in paraffin wax, cut in 3 µm thick sections, mounted on glass slides, stained with haematoxylin and eosin, and cover slipped according to standard procedures.[21]

2.5 *In vitro evaluation*

2.5.1 Bacteria preparation

Sample tubes containing overnight cultures of *S. aureus*, *S. epidermidis*, and *S. agalactiae*, as well as CyMol® fixated aliquots of the same bacteria, were pelleted by centrifugation and re-suspended in 3% skimmed milk powder in phosphate buffered saline (MPBS) and incubated for 15 min on ice. This procedure was repeated twice for pre-blocking to reduce subsequent non-specific binding of TAMRA-K-A9 to the cells. Each of the cell samples were split in two vials: fluorescence sample and control sample, and pelleted by centrifugation.

2.5.2 Morphological binding study

Table 3 shows the experimental setup for the *in vitro* binding evaluation of the custom synthesised TAMRA-K-A9, which was performed after the mice pilot infection study of [^{68}Ga]Ga-DOTA-K-A9, to further characterise the bacterial binding of the A9 peptide.

100 µg (53 nmol) of TAMRA-K-A9 was dissolved in 3% MPBS (1 ml) and the cells in the fluorescence sample vials were re-suspended in this 0.05 mM TAMRA-K-A9 solution (100 µl), while the cells in the control sample vials were re-suspended in 3% MPBS (100 µl). All vials were incubated in the dark for 1 h at room temperature. The cells were subsequently

washed once in 0.1% Tween-20 in PBS and twice in PBS and stored on ice until microscopy. The membrane-impermeable DNA-binding stain, TOTO®-1, was added to selected vials in a working concentration of 0.001 mM (Table 3). This was performed to identify if TAMRA-K-A9 preferentially bound to (dead) cells with a permeable membrane, indicating an intracellular target. All samples were visualised on a Zeiss Axiovert 200 M epifluorescence microscope (Göttingen, Germany), using a filter set 43 for TAMRA-K-A9 and filter set 10 for TOTO®-1.

3 Results and discussion

3.1 *Radiochemistry*

The initial gallium-68 labelling method (Section 2.3.1) yielded 928 ± 70 MBq [^{68}Ga]Ga-DOTA-K-A9 in >91% radiochemical purity with a molar activity of 27 ± 2.0 GBq/μmol at end of synthesis, and a stability of 2 h in the product formulation (pH 3.9 - 4.1). In this method, the HEPES is necessary in the product formulation where it acts as radical scavenger[22,23] to prevent radiolysis of the radio-peptide. In a previous evaluation of the A9 ^{68}Ga-labelling, the use of HEPES aq. solutions lower than 0.1 M, resulted in a slightly improved radiochemical purity, potentially due to reduced [^{68}Ga]Ga-HEPES complexation, while the stability of [^{68}Ga]Ga-DOTA-K-A9 deceased most likely as a consequence of increased radiolysis.[18]

The acetone content in the formulation when applying the initial gallium-68 labelling method necessitated extensive dilution prior to the *in vivo* injection, thus limiting the radioactivity dose given to the mice in the pilot study. Consequently, an optimised preparation method omitting the use of acetone was developed (Section 2.3.2), yielding 371 ± 51 MBq [^{68}Ga]Ga-DOTA-K-A9 in 93 ± 0.9% radiochemical purity with a molar activity of 10 ± 1.4 GBq/μmol at end of synthesis and a stability up to 2 h in the product formulation (pH 5.1-5.7) (Table 4).

Compared to the initial method, the lower yield and thus molar activity of the optimised method is partly due to a lower starting activity of [^{68}Ga]$GaCl_3$ applied, but also a consequence of radioactivity lost during the product purification step.

As we have reported for another dodecapeptide [^{68}Ga]Ga-DOTA-KGSG-A11, the change of the eluent from the HCl/acetone solution to the hypertonic NaCl/HCl solution in the pre-purification of the gallium-68 eluate resulted in an increase in secondary silanol interaction between the cationic peptide [^{68}Ga]Ga-DOTA-K-A9 and the C18 purification cartridge. This phenomenon was further investigated through additional purification experiments with [^{68}Ga]Ga-DOTA-K-A9, applying different solutions for the pre-conditioning and elution of the C18 cartridges (Table 5).

As seen in the first line of Table 5, when employing the traditional purification setup: C18 cartridge pre-conditioning with first a 50% EtOH aq. solution then isotonic saline; product rinse by isotonic saline; and final a product elution with first a 50% EtOH aq. solution followed by isotonic saline for formulation, half of the radioactivity remained on the C18-cartridge, including retained [^{68}Ga]Ga-DOTA-K-A9. During the investigation of the similar issue with [^{68}Ga]Ga-DOTA-KGSG-A11 on the C18 cartridge, we observed no improvement in the elution of the radio-peptide when increasing the ethanol concentration in the product elution step.[18] However, the [^{68}Ga]Ga-DOTA-KGSG-A11 peptide was most efficiently eluted when using a 50% EtOH/PBS (2%) solution as eluent and the radio-peptide was subsequently stable in that formulation up to 2 h. Therefore, when evaluating the [^{68}Ga]Ga-DOTA-K-A9 purification we also tried a few different setups with both a 50% EtOH/PBS (2%) solution pH 6.5 and a 50% EtOH/0.1 M HEPES aq. solution pH 6.5 as the eluents (Table 5), which likewise resulted in an efficient elution [^{68}Ga]Ga-DOTA-K-A9 in the activity rage of 514 ± 93 MBq. Nevertheless, unlike the [^{68}Ga]Ga-DOTA-KGSG-A11 peptide, the [^{68}Ga]Ga-DOTA-K-A9 peptide was not stable in formulations of PBS pH 6.5.[18] And additionally the

[^{68}Ga]Ga-DOTA-K-A9 also appeared to be less stable in the HEPES/ethanol formulations (pH 5.3-6.5) with the radiochemical purity decreasing from around 94% to 80% after 2 hours. A possible explanation for this difference in stability of the two compounds is most likely found in the peptide sequences and not necessarily a consequence of radiolysis; the activity range (514 ± 93 MBq) of the product in the HEPES/ethanol formulations (pH 5.3 - 6.5) was lower than the product activity range (928 ± 70 MBq) in the initial ^{68}Ga-labelling method with the 0.1 M HEPES aq. formulation (pH 3.9 - 4.1). When comparing the peptides A9 (TDGRRYSSGAMR) and A11 (DVGRRFSSASTR) they have a 50% identical amino acid sequence with a few additional positions with small difference between the residues e.g. phenylalanine and tyrosine. Despite the similarities, the A9-K-DOTA peptide contains an aspartic acid residue placed next to a glycine, as well as a methionine residue, thereby making it more susceptible to both hydrolysis and oxidation influenced by pH. However, only a few experiments was performed employing HEPES/ethanol in the product formulation and the issue was not further investigated, since the aim of the study was the *in vivo* evaluation of [^{68}Ga]Ga-DOTA-K-A9. Consequently, an intermediate solution with a purification method applying a 0.1 M HEPES aq. solution pH 5.2 for both the C18 cartridge pre-conditioning and product rinse, and a 50% EtOH aq. solution as the cartridge eluent was chosen for the preparation of [^{68}Ga]Ga-DOTA-K-A9.

3.2 *In vivo evaluation*

3.2.1 Model characterisation

The murine SC *S. aureus* infection model with µPET/MRI analysis 24 h post-inoculation was chosen to obtain an acute inflammatory response with incipient abscess formation, containing both dead and viable bacteria.[16,22] The inflammation model was added to evaluate if the imaging agent was able to distinguish between host tissue inflammatory lesions and bacterial

infection. Of the two methods typically utilised for creating an inflammation model i.e. injection of heat killed bacteria[23-25] or turpentine oil,[26-28] the latter method was chosen to gain supplement information about tracer accumulation in sterile inflammatory lesions absent of bacteria or bacterial components. The same post-inoculation time was applied for the turpentine induced inflammation in mice to align the inflammatory responses of the sterile and infectious tissue lesions.

To compare the two lesion types, histopathology and microbiology analyses were performed post-mortem (Table 2). Biopsies from 6 turpentine and 3 *S. aureus* inoculated mice were examined histologically. Various tissue elements, e.g. fatty tissue (white and occasionally brown), sweat glands, striated muscle fibres, lymph nodes, and occasionally skin (epidermis and dermis), were present, often in irregular arrangement, due to multi-purpose use of biopsies (Table 2). All biopsies showed presence of acute haemorrhage, and expressed similar inflammatory changes. These consisted of areas of oedema (occasionally containing fibroblast- or macrophage-like cells, and degranulated mast cells), and areas of accumulated neutrophils related to fatty tissue or striated muscle fibres, often being necrotic. In addition, two of the *S. aureus* injected mice (No. 16 and 17) had microcolonies of coccoid bacteria located central in necrotic tissue, which was marginated by neutrophils (Figure 3). No viable bacteria were located in the tissue sample of the *S. aureus* injected mouse No. 13 in Table 2. This was most likely due to the combination of heterogeneous bacterial distribution and division of the abscess tissue for both histopathology and microbiology analyses. To avoid this potential problem all other tissue samples from the µPET scanned *S. aureus* infection mice solely went to microbiology analysis, while two additional mice (No. 16 and 17) were applied to histologically characterise the infection model (Table 2). The microbiological analysis confirmed the aseptic environment in the turpentine inflammation model with no CFU grown from the lesions, while in the *S. aureus* infection model all animals had a clinical

distinct abscess formation and all but one of the abscesses contained viable bacteria with an average bacterial load of 6.1 ± 1.1 log CFU (Table 2).

3.2.2 Excretion

In the previously reported *in vitro* and *in vivo* studies, [^{68}Ga]Ga-DOTA-K-A9 showed a preserved binding towards *S. aureus* after gallium-68 labelling and desirable biodistribution features, although it showed a relatively fast metabolic degradation *in vivo*; with 40% of the remaining radioactivity in the blood after 15 min corresponding to [^{68}Ga]Ga-DOTA-K-A9.[18] In this study the µPET scans of the mice, no physiological accumulation of [^{68}Ga]Ga-DOTA-K-A9 was observed in gastrointestinal system, including biliary duct, gall bladder, or intestine. Thus, the radiolabelled peptide seemed to be solely excreted by the urinary system. Furthermore, when compared to the [^{18}F]FDG no physiological accumulation was seen in the bowel and heart. Table 6 shows the radioactivity distribution in the urinary system based on the time-activity curves generated from the dynamic [^{68}Ga]Ga-DOTA-K-A9 µPET scan (Figure 4). The accumulation in the kidneys peaked after 2.5 min with 8.1% ± 0.7% of the injected dose located in one kidney after which the activity decreases. Excretion to the urine was fast with 55.9% ± 4.1% of the whole body activity being in the urinary bladder 15 min post-injection. After 60 min 84.5% ± 1.2% of the activity on the PET image was found in the urinary bladder, with the remaining accumulation primarily being located in the kidneys and the infectious and inflammatory foci.

3.2.3 Infection and inflammation binding study

The results of the µPET/MRI experiments of [^{68}Ga]Ga-DOTA-K-A9 and [^{18}F]FDG in mice (n = 15) with SC infection are shown in Table 2. In the infection mice of the pilot study (n = 3) accumulation in the infected foci was observed for both [^{68}Ga]Ga-DOTA-K-A9 and

[^{18}F]FDG with the target to background ratios being 1.89 ± 0.88 and 4.24 ± 2.36, respectively. Figure 5 illustrates the µPET/MRI scans at 60 - 90 min, in which the [^{68}Ga]Ga-DOTA-K-A9 was primarily localised in the infected abscess and the urinary bladder. The substantial difference between the injected [^{68}Ga]Ga-DOTA-K-A9 and [^{18}F]FDG doses, 3.2 ± 1.5 MBq and 11.7 ± 7.3 MBq, respectively, was a consequence of high acetone content in the [^{68}Ga]Ga-DOTA-K-A9 product formulation, when employing the initial gallium-68 labelling method (Section 2.3.1), necessitating an additional pre-injection saline dilution. In the case of one mouse, the injected dose of 1.5 MBq yielded too poor image quality to allow proper data analysis.

After the µPET scans of the mice in the pilot infection study confirmed an *in vivo* accumulation of [^{68}Ga]Ga-DOTA-K-A9 in the infected foci despite a fast renal clearance, the study was expanded with additional 12 mice to investigate the ability of the tracer to distinguish sterile inflammation from infection. The synthesis of [^{68}Ga]Ga-DOTA-K-A9 was optimised, as described in Section 2.3.2, and the scan protocol was additionally adjusted by reducing the µPET scan time from 100 min to 60 min according to Figure 2 enabling the evaluation of 4 mice on one day. The mice (n = 12) in the infection and inflammation comparison study received doses of [^{68}Ga]Ga-DOTA-K-A9 and [^{18}F]FDG in the same range with a slightly higher amount of [^{18}F]FDG given when possible, due to a 60 min post-injection delay of the [^{18}F]FDG scan. The results of the µPET/MRI scans showed that [^{68}Ga]Ga-DOTA-K-A9 accumulated in both infectious (Figure 6) and sterile inflammatory foci (Figure 7), thus not being bacteria-specific. Furthermore, comparing the accumulation in lesion and contra-lateral subcutis a higher ratio was found in inflammation compared to infection with 3.64 ± 1.08 and 2.45 ± 0.44, respectively, though this tendency was also observed for [^{18}F]FDG (Table 2). In comparison to [^{18}F]FDG, the [^{68}Ga]Ga-DOTA-K-A9 did accumulate in all the infected mice at injected doses ≥3.6 MBq, whereas [^{18}F]FDG had two

false negative scans for infection. Although, a high physiological uptake of [^{18}F]FDG was seen in brown adipose tissue of some mice, this did not significantly interfere with the image analysis.

The accumulation of [^{68}Ga]Ga-DOTA-K-A9 in both sterile inflammation and infection indicates that factors of the inflammatory response are involved in the uptake. The cationic properties of the A9 peptide could potentially have contributed to the uptake mechanism *in vivo* through electrostatic interactions with negatively charged components of dead bacterial cells and damaged necrotic host tissue cells. This binding pattern has previously been described in the evaluation of bacterial membrane-binding imaging agents, such as ubiquicidin and bis-dipicolylamine-zinc[2,3,29,30], where cationic domains in the tracers bound to negatively charged molecules in the bacterial membrane. In the case of bis-dipicolylamine, the binding also included negatively charged structures becoming accessible through bacterial cell lysis and/or disruption of plasma membrane in mammalian cells during necrosis. However, the lysed material from bacteria and host tissue cells would need to be locally present in large excess to avoid blocking by unlabelled A9 peptide.

3.3 *In vitro* evaluation

The A9 peptide was originally selected by phage-display towards a *S. aureus* biofilm, but it was not evident to what extent the binding was occurring towards viable or dead bacteria or even the biofilm matrix; the imaging probe [^{68}Ga]Ga-DOTA-K-A9 was, however, subsequently confirmed to bind to both Gram-positive and negative bacteria *in vitro*.[18] That previously reported experiment was performed on bacteria grown overnight, but as no subsequent microbiological analyses were performed to confirm the viability of the bacteria, it was not known if the observed binding necessitated living bacteria. To clarify this, the binding of the fluorescence analogue TAMRA-K-A9 was evaluated *in vitro* towards

S. aureus and two other bacterial strains often associated with prosthesis related infections (Table 3) to investigate if the accumulation observed in the murine infections was selective to viable or dead bacteria. However, only few cells in fresh cultures bound the probe (Figure 8A, 8D, and 8G). This led us to hypothesise that the target was intracellular and therefore only accessible in cells with a compromised membrane. The membrane-impermeable DNA stain TOTO®-1 was therefore combined with TAMRA-K-A9 to assess membrane integrity, and we confirmed that TAMRA-K-A9 only bound to cells with a compromised membrane (Figure 8C, 8F). To further corroborate this conclusion, we evaluated the binding of TAMRA-K-A9 in samples of dead bacteria and confirmed that nearly all bacteria in these samples bound the probe (Figure 8B, 8E, and 8H). Additionally, the binding was not confined to *S. aureus* but occurred with all the bacterial species tested (Table 3). Altogether, the results indicated that TAMRA-K-A9 binds to an intracellular epitope in dead bacteria with permeable membranes, and that the epitope were present in all bacterial species tested. Although, both [^{68}Ga]Ga-DOTA-K-A9 (Figure 1A) and TAMRA-K-A9 (Figure 1B) are based on the same binding pharmacophore, i.e. the A9 peptide, it cannot be completely disregarded that the individual imaging moiety could somehow influence their affinity differently. However, as the A9 peptide was initially selected towards a *S. aureus* biofilm, i.e. aggregated viable and dead bacteria embedded in self-produced matrix, the identified affinity of the peptide towards an intracellular epitope in dead bacteria is explicable.

4 Conclusion

The *in vivo* study did not show selectivity of [^{68}Ga]Ga-DOTA-K-A9 towards infection, as the tracer accumulated in mice with both infection and turpentine induced inflammation and it is therefore not applicable as a bacteria-specific imaging agent. However, The [^{68}Ga]Ga-DOTA-K-A9 tracer was able to detect low levels of inflammation with limited background

uptake on the same level as [^{18}F]FDG. The lesion localisation of [^{68}Ga]Ga-DOTA-K-A9 in the murine sterile inflammation model prove that the accumulation of the imaging agent occurs due to factors associated with the inflammatory response, which may include increased blood flow, membrane permeability, as well as the host inflammatory cells. And since the previous *in vitro* results showed binding of [^{68}Ga]Ga-DOTA-K-A9 towards *S. aureus*,[18] while the present study identified a binding of the fluorescence analogue TAMRA-K-A9 to an intracellular epitope in dead bacteria with permeable membranes. The uptake is presumably a combination of local hyperaemia, vascular leakiness and/or binding to an epitope present in dead bacteria and inflammatory cells potentially by electrostatic interactions of the cationic A9 peptide.

In the continued search of potential infection-specific PET tracers we still regard the selection process by phage-display as a valuable tool to identify peptides with a selective binding affinity to bacterial components.

Acknowledgements

The research was funded by the Danish Council for Independent Research, Technology, and Production Sciences, grant No. 0602-01911B (11-107077) and further supported by The Danish Agency for Science, Technology and Innovation, grant No. 0604-00205B/09-052174 and related result contracts. The authors are grateful to Mette Simonsen and Jonas Brorson at the Department of Nuclear Medicine and PET-centre, Aarhus University Hospital for assisting in the mice experiments.

Conflict of Interest

The authors declare that they have no conflict of interest.

Reference List

1. Bunschoten A, Welling MM, Termaat MF, Sathekge M, van Leeuwen FW. Development and prospects of dedicated tracers for the molecular imaging of bacterial infections. Bioconjug Chem. 2013;24(12):1971-89.

2. Rice DR, Plaunt AJ, Turkyilmaz S, Smith M, Wang Y, Rusckowski M, et al. Evaluation of [(111)In]-labeled zinc-dipicolylamine tracers for SPECT imaging of bacterial infection. Mol Imaging Biol. 2015;17(2):204-13.

3. van Oosten M, Hahn M, Crane LM, Pleijhuis RG, Francis KP, van Dijl JM, et al. Targeted imaging of bacterial infections: advances, hurdles and hopes. FEMS Microbiol Rev. 2015;Review article:1-25.

4. Ady J, Fong Y. Imaging for infection: from visualization of inflammation to visualization of microbes. Surg Infect (Larchmt). 2014;15(6):700-7.

5. Goldsmith SJ, Vallabhajosula S. Clinically proven radiopharmaceuticals for infection imaging: mechanisms and applications. Semin Nucl Med. 2009;39(1):2-10.

6. Heuker M, Gomes A, van Dijl JM, van Dam GM, Friedrich AW, Sinha B, et al. Preclinical studies and prospective clinical applications for bacteria-targeted imaging: the future is bright. Clin Transl Imaging. 2016;4:253-64.

7. Britton KE, Wareham DW, Das SS, Solanki KK, Amaral H, Bhatnagar A, et al. Imaging bacterial infection with (99m)Tc-ciprofloxacin (Infecton). J Clin Pathol. 2002;55(11):817-23.

8. Langer O, Brunner M, Zeitlinger M, Ziegler S, Muller U, Dobrozemsky G, et al. In vitro and in vivo evaluation of [(18)F]ciprofloxacin for the imaging of bacterial infections with PET. Eur J Nucl Med Mol Imaging. 2005;32(2):143-50.

9. Sarda L, Cremieux AC, Lebellec Y, Meulemans A, Lebtahi R, Hayem G, et al. Inability of (99m)Tc-ciprofloxacin scintigraphy to discriminate between septic and sterile osteoarticular diseases. J Nucl Med. 2003;44(6):920-6.

10. Akhtar MS, Qaisar A, Irfanullah J, Iqbal J, Khan B, Jehangir M, et al. Antimicrobial peptide (99m)Tc-ubiquicidin 29-41 as human infection-imaging agent: clinical trial. J Nucl Med. 2005;46(4):567-73.

11. Nibbering PH, Welling MM, Paulusma-Annema A, Brouwer CP, Lupetti A, Pauwels EK. (99m)Tc-Labeled UBI 29-41 peptide for monitoring the efficacy of antibacterial agents in mice infected with Staphylococcus aureus. J Nucl Med. 2004;45(2):321-6.

12. Sarda-Mantel L, Saleh-Mghir A, Welling MM, Meulemans A, Vrigneaud JM, Raguin O, et al. Evaluation of (99m)Tc-UBI 29-41 scintigraphy for specific detection of experimental Staphylococcus aureus prosthetic joint infections. Eur J Nucl Med Mol Imaging. 2007;34(8):1302-9.

13. Vilche M, Reyes AL, Vasilskis E, Oliver P, Balter H, Engler H. (6)(8)Ga-NOTA-UBI-29-41 as a PET Tracer for Detection of Bacterial Infection. J Nucl Med. 2016;57(4):622-7.

14. Ning X, Seo W, Lee S, Takemiya K, Rafi M, Feng X, et al. PET imaging of bacterial infections with fluorine-18-labeled maltohexaose. Angew Chem Int Ed Engl. 2014;53(51):14096-101.

15. Li J, Zheng H, Fodah R, Warawa JM, Ng CK. Validation of 2-(18)F-Fluorodeoxysorbitol as a Potential Radiopharmaceutical for Imaging Bacterial Infection in the Lung. J Nucl Med. 2018;59(1):134-9.

16. Otto M. Staphylococcal infections: mechanisms of biofilm maturation and detachment as critical determinants of pathogenicity. Annu Rev Med. 2013;64:175-88.

17. Boellaard R, Delgado-Bolton R, Oyen WJG, Giammarile F, Tatsch K, Eschner W, et al. FDG PET/CT: EANM procedure guidelines for tumour imaging: version 2.0. Eur J Nucl Med Mol Imaging. 2015;42(2):328-54.

18. Nielsen KM, Kyneb MH, Alstrup AK, Jensen JJ, Bender D, Schonheyder HC, et al. 68Ga-labeled phage-display selected peptides as tracers for positron emission tomography imaging of Staphylococcus aureus biofilm-associated infections: Selection, radiolabelling and preliminary biological evaluation. Nucl Med Biol. 2016;43(10):593-605.

19. Nielsen KM. Design of a multi-functional automated (68)Ga-synthesis program. J Labelled Comp Radiopharm ISRS 2015; 5/15/20152015. p. S395.

20. Mueller D, Klette I, Baum RP, Gottschaldt M, Schultz MK, Breeman WA. Simplified NaCl based (68)Ga concentration and labeling procedure for rapid synthesis of (68)Ga radiopharmaceuticals in high radiochemical purity. Bioconjug Chem. 2012;23(8):1712-7.

21. Gamble M. The Hematoxylins and Eosin. In: Bancroft JD, Gamble M, editors. Theory and Practice of Histological Techniques. 6 ed: Churchill Livingstone Elsevier; 2008. p. 121-34.

22. Lowy FD. Staphylococcus aureus infections. N Engl J Med. 1998;339(8):520-32.

23. Weinstein EA, Ordonez AA, DeMarco VP, Murawski AM, Pokkali S, MacDonald EM, et al. Imaging Enterobacteriaceae infection in vivo with (18)F-fluorodeoxysorbitol positron emission tomography. Sci Transl Med. 2014;6(259):259ra146.

24. Essouissi I, Ghali W, Saied NM, Saidi M. Synthesis and evaluation of (99m)Tc-N-sulfanilamide ferrocene carboxamide as bacterial infections detector. Nucl Med Biol. 2010;37(7):821-9.

25. Hina S, Rajoka MI, Roohi S, Haque A, Qasim M. Preparation, biodistribution, and scintigraphic evaluation of (99m)Tc-clindamycin: an infection imaging agent. Appl Biochem Biotechnol. 2014;174(4):1420-33.

26. Martinez ME, Kiyono Y, Noriki S, Inai K, Mandap KS, Kobayashi M, et al. New radiosynthesis of 2-deoxy-2-[(18)F]fluoroacetamido-D-glucopyranose and its evaluation as a bacterial infections imaging agent. Nucl Med Biol. 2011;38(6):807-17.

27. Ebenhan T, Zeevaart JR, Venter JD, Govender T, Kruger GH, Jarvis NV, et al. Preclinical evaluation of (68)Ga-labeled 1,4,7-triazacyclononane-1,4,7-triacetic acid-ubiquicidin as a radioligand for PET infection imaging. J Nucl Med. 2014;55(2):308-14.

28. Nayak DK, Baishya R, Halder KK, Sen T, Sarkar BR, Ganguly S, et al. Evaluation of (99m)Tc(I)-tricarbonyl complexes of fluoroquinolones for targeting bacterial infection. Metallomics. 2012;4(11):1197-208.

29. Thakur ML, Zhang K, Paudyal B, Devakumar D, Covarrubias MY, Chen CP, et al. Targeting apoptosis for optical imaging of infection. Mol Imaging Biol. 2012;14(2):163-71.

30. Ferro-Flores G, Arteaga de MC, Pedraza-Lopez M, Melendez-Alafort L, Zhang YM, Rusckowski M, et al. In vitro and in vivo assessment of (99m)Tc-UBI specificity for bacteria. Nucl Med Biol. 2003;30(6):597-603.

Table 1: Bacteria applied in the evaluation of the [^{68}Ga]Ga-DOTA-K-A9 and TAMRA-K-A9 peptides

ID	Species	Reference No.	Source	Application
S. aureus (130858)	*Staphylococcus aureus*	2011-130858	Human synovial fluid[a]	Murine SC infection *In vitro* binding study
S. epidermidis	*Staphylococcus epidermidis*	DSM 1798	Culture collection	*In vitro* binding study
S. agalactiae	*Streptococcus agalactiae*	NCTC 11078	Culture collection	*In vitro* binding study

All bacteria were stored at -80 °C. DSM: Deutsche Sammlung von Mikroorganismen, Braunschweig, Germany. NCTC: National Collection of Type Cultures, Salisbury, UK. a) Knee prosthesis patient at the Department of Clinical Microbiology, Aalborg University Hospital, Denmark.

Table 2: Results of the [^{68}Ga]Ga-DOTA-K-A9 µPET/MRI scans and post-mortem analyses of murine subcutaneous infection and inflammation models

Mice No	Model Type	First scan time post-inoculation (hours)	Intravenous injected dose (MBq)		Time between scans (hours)	Target/background ratios on µPET				Post-mortem analyses	
						Lesion/ lateral subcutis		Lesion/ shoulder muscle		Microbiology (log CFU)	Histology confirm
			[^{68}Ga]Ga-DOTA-K-A9	[^{18}F]FDG		[^{68}Ga]Ga-DOTA-K-A9	[^{18}F]FDG	[^{68}Ga]Ga-DOTA-K-A9	[^{18}F]FDG		
1	Infection	≥24	4.3	19.9	≥5	1.91	6.90	n/a	n/a	6.6	n/a
2	Infection	≥24	1.5	6.2	≥5	1.00 [a]	3.40	n/a	n/a	6.8	n/a
3	Infection	≥24	3.8	8.9	≥5	2.75	2.42	n/a	n/a	6.4	n/a
Mean ± SD			3.2 ± 1.5	11.7 ±7.3		1.89 ± 0.88	4.24 ± 2.36			6.6 ± 0.2	
4	Inflammation	25.0	11.5	18.9	6.25	3.31	3.31	4.24	5.22	0.0	Yes
5	Inflammation	26.6	3.6 [b]	4.6	6.05	3.31	3.53	2.86	4.28	0.0	Yes
6	Inflammation	29.7	8.6	9.4	n/a [g]	3.80	n/a [g]	4.40	n/a [g]	0.0	Yes
7	Inflammation	25.1	9.5	7.6	5.88	n/a [f]	1.00	n/a [f]	1.00	0.0	Yes
8	Inflammation	26.5	4.1	12.2	5.92	2.43	1.00	3.85	1.00	0.0	Yes
9	Inflammation	28.0	10.4	9.0	5.70	5.37	2.91 [c]	4.67	1.66 [c]	0.0	Yes
Mean ± SD		26.8 ± 1.8	8.0 ± 3.3	10.3 ± 4.9	358 ± 12	3.64 ± 1.08	2.35 ± 1.25	4.00 ± 0.71	2.63 ± 1.98	0.0 ± 0.0	
10	Infection	29.3	4.3	6.3	5.72	2.15	1.00	2.69	1.00	4.4	n/a [e]
11	Infection	24.1	10.2	12.6	9.03	2.20	2.27 [c]	3.16	2.02 [c]	0.0 [d]	n/a [e]
12	Infection	25.5	4.8	9.7	9.25	2.57	1.00 [c]	4.49	1.00 [c]	5.9	n/a [e]
13	Infection	28.1	7.7 [h]	n/a	n/a	n/a	n/a	n/a	n/a	7.1	Yes
14	Infection	30.0	9.7 [b]	6.6	n/a [g]	2.15	n/a [g]	2.69	n/a [g]	7.0	n/a [e]
15	Infection	31.8	3.7	4.5	4.62	3.16	2.74 [c]	4.97	2.21 [c]	6.0	n/a [e]
Mean ± SD		28.1 ± 2.9	6.7 ± 2.9	7.9 ± 3.2	429 ± 140	2.45 ± 0.44	1.75 ± 0.69	3.60 ± 1.06	1.56 ± 0.65	6.1 ± 1.1	
16	Infection	Mice applied for histological characterization of the infection model									Yes
17	Infection										Yes

For mice No. 1-3 in the pilot study the µPET scans are summed from 60-90 min, while for mice No. 4-15 the scans are summed from 30-60 min. a) The injected dose of [^{68}Ga]Ga-DOTA-K-A9 yielded too poor image quality to allow proper data analysis. b) Paravenous injection of the tracer. c) High physiological uptake in brown adipose tissue. d) No bacteria were grown from this tissue abscess, thus not included in the mean ± SD calculation. e) Histology was not performed to avoid dividing the abscess. f) Image analysis not possible, due to artefact from retrograde leakage of injected tracer. g) The anesthetised mouse died shortly after [^{18}F]FDG injection. h) The anesthetised mouse died during the µPET scan. n/a: not available, either the analyses were not performed or the results are not available for various reasons (e-h).

Table 3: Experimental setup and results of the *in vitro* binding evaluation of TAMRA-K-A9 on various bacteria

Bacteria		Sample content	Microscopy results	Figure
S. aureus	Viable	TAMRA-K-A9 & added TOTO®-1	Uptake of TAMRA-K-A9 in very few cells The uptake is almost exclusively in dead bacteria	8A 8C
		MPBS	No fluorescence	
	Dead	TAMRA-K-A9	Higher uptake of TAMRA-K-A9 compared to *S. aureus* viable cell test	8B
		MPBS	No fluorescence	
S. agalactiae	Viable	TAMRA-K-A9 & added TOTO®-1	Uptake of TAMRA-K-A9 in more cells compared to viable *S. aureus* The uptake is only in dead bacteria	8D 8F
		MPBS	No fluorescence	
	Dead	TAMRA-K-A9	Higher uptake of TAMRA-K-A9 compared to S. agalactiae viable cell test	8E
		MPBS	No fluorescence	
S. epidermidis	Viable	TAMRA-K-A9	Uptake of TAMRA-K-A9 in very few cells as seen with *S. aureus*	8G
		MPBS	No fluorescence	
	Dead	TAMRA-K-A9	Uptake of TAMRA-K-A9 in all the dead bacteria	8H
		MPBS	No fluorescence	

MPBS: skimmed milk powder in PBS. TOTO®-1: a membrane-impermeable DNA-binding stain. Negative control samples were only added MPBS.

Table 4: Stability of the [^{68}Ga]Ga-DOTA-K-A9 peptide in product formulations after purification

Product formulation (pH 5.1-5.7)		Time points	[^{68}Ga]Ga-DOTA-K-A9
Radiochemical purity	TLC	EOS	99% ± 0.5%
	HPLC	EOS	93% ± 0.8%
		1 h	91% ± 1.0%
		2.5 h	90% ± 0.5%

EOS: End of synthesis. Results are given as mean ± SD, n ≥ 3.

Table 5: Optimisation of [^{68}Ga]DOTA-K-A9 purification on C18-light cartridge

Purification methods			N	% of starting radioactivity			Radiochemical purity Product (%)
Pre-condition	Product rinse	Product elution		C18 waste	C18 cartridge	Product	
1. 50% EtOH/H_2O **2.** Isotonic saline	Isotonic saline	**1.** 1 ml 50% EtOH/H_2O **2.** 5 ml isotonic saline	5	1.05 ± 0.35	51.3 ± 12.0	33.4 ± 13.1	91.8 ± 0.5
1. 50% EtOH/PBS pH 6.5 **2.** Isotonic saline	Isotonic saline	**1.** 1 ml 50% EtOH/PBS pH 6.5 **2.** Isotonic saline	1	0.60	2.80	84.0	88
1. 50% EtOH/ 0.1 M HEPES pH 6.5 **2.** Isotonic saline	Isotonic saline	**1.** 1 ml 50% EtOH/0.1 M HEPES pH 6.5 **2.** Isotonic saline	1	0.97	5.97	80.8	94
1. 50% EtOH/H_2O **2.** 0.1 M HEPES pH 6.5	0.1 M HEPES pH 6.5	**1.** 1 ml 50% EtOH/H_2O **2.** 0.1 M HEPES pH 6.5	1	0.63	5.86	81.9	94
Combined for 0.1 M HEPES and PBS at pH 6.5			3	0.73 ± 0.21	4.88 ± 1.80	82.2 ± 1.64	92.0 ± 3.5
1. 50% EtOH/H_2O **2.** 0.1 M HEPES pH 5.2	0.1 M HEPES pH 5.2	**1.** 1 ml 50% EtOH/H_2O **2.** 0.1 M HEPES pH 5.2	1	1.03	23.5	58.9	95
1. 50% EtOH/H_2O **2.** 0.1 M HEPES pH 5.2	0.1 M HEPES pH 5.2	**1.** 1 ml 50% EtOH/H_2O **2.** Isotonic saline	8	1.40 ± 0.38	28.8 ± 5.04	55.7 ± 3.61	92.9 ± 0.8
Combined for 0.1 M HEPES at pH 5.2			9	1.36 ± 0.37	28.2 ± 5.03	56.1 ± 3.54	93.1 ± 1.1

N: number of occurrences. PBS: sodium phosphate (2%) in saline. Radiochemical purity: Measured by radio-HPLC at end of synthesis. Gallium-68 colloid ≤1% measured by radio-TLC. The radioactivity is decay corrected.

Table 6: Radioactivity distribution in the murine urinary system from time-activity curves during [^{68}Ga]Ga-DOTA-K-A9 µPET scan

Time post-injection	% of the whole body radioactivity	
	Left kidney	Urinary bladder
2.5 min	8.06 ± 0.70	18.51 ± 3.84
5.0 min	2.52 ± 0.30	32.46 ± 4.32
15 min	3.11 ± 0.21	55.88 ± 4.12
25 min	2.07 ± 0.07	68.88 ± 3.10
40 min	1.40 ± 0.12	78.18 ± 2.07
60 min	0.97 ± 0.12	84.54 ± 1.17

Results are given as mean ± SD and based on mice No. 6, 9, 12, and 15 in Table 2.

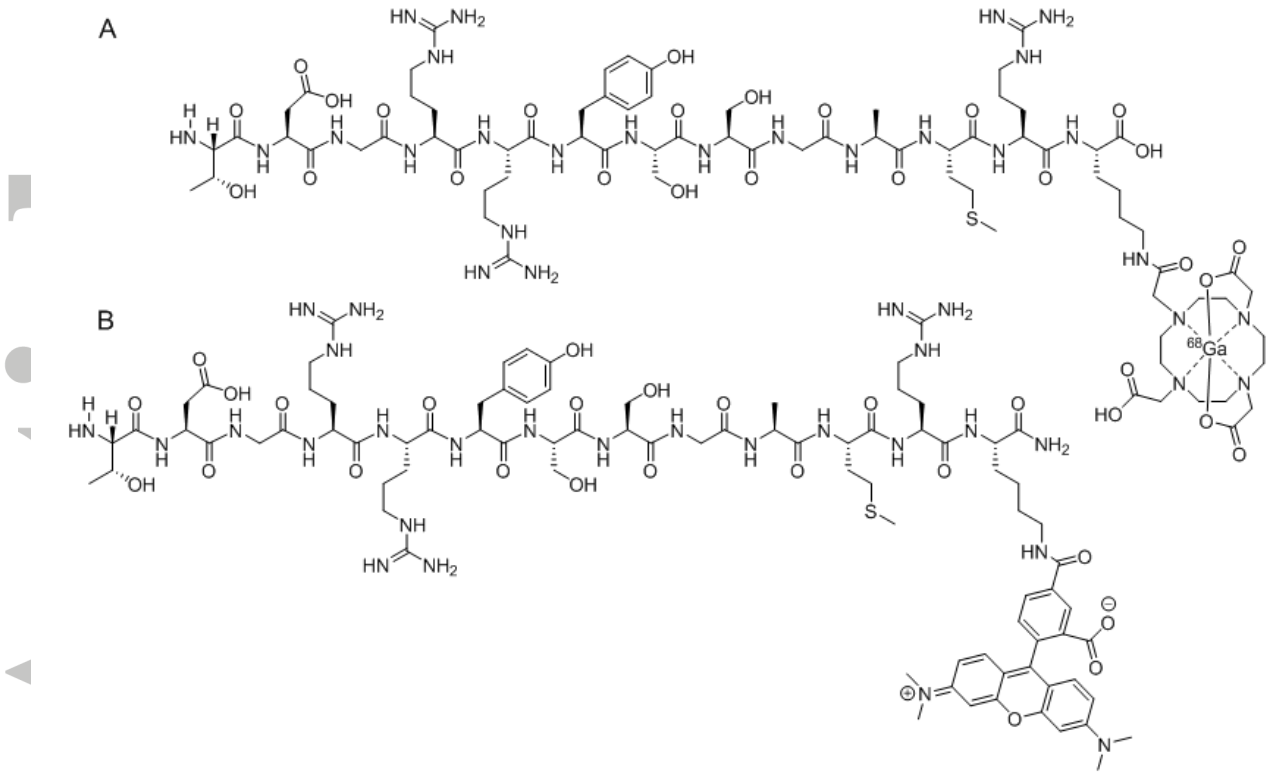

Figure 1: Molecular structure of (A) the radiolabelled peptide [^{68}Ga]Ga-DOTA-K-A9 (1937 Da) and (B) the fluorescence analogue TAMRA-K-A9 (1896 Da). In the two compounds, the A9 peptide, TDGRRYSSGAMR, are supplied with an imaging moiety, [^{68}Ga]Ga-DOTA or TAMRA, respectively, conjugated through an additional lysine residue at the C-terminal. The C-terminal is not believed to participate in the binding as it was connected to the phage particle in the preceding selection experiments.

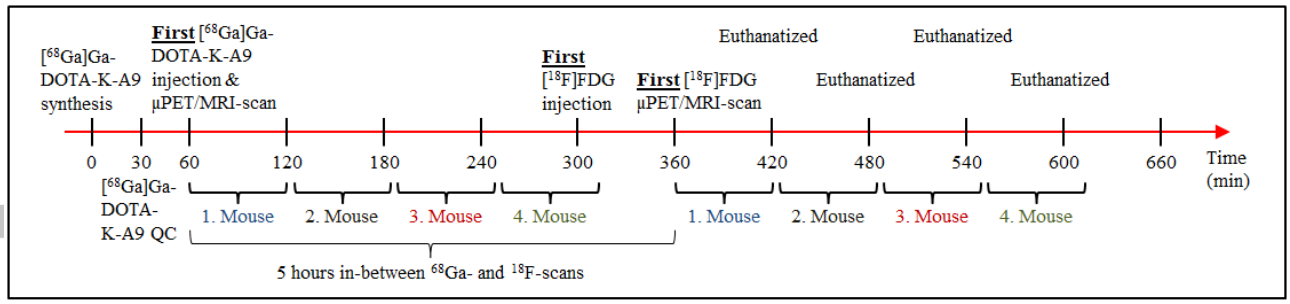

Figure 2: Illustration of the mice scans timeline in the main comparison study. The scan protocol was optimized from the pilot study, by reducing the µPET-scan time from 100 to 60 min facilitating up to four consecutive [^{68}Ga]Ga-DOTA-K-A9 µPET/MRI scans, prior to the following [^{18}F]FDG µPET/MRI scan of each mouse five hours later. In this study setup, four mice was evaluated a day.

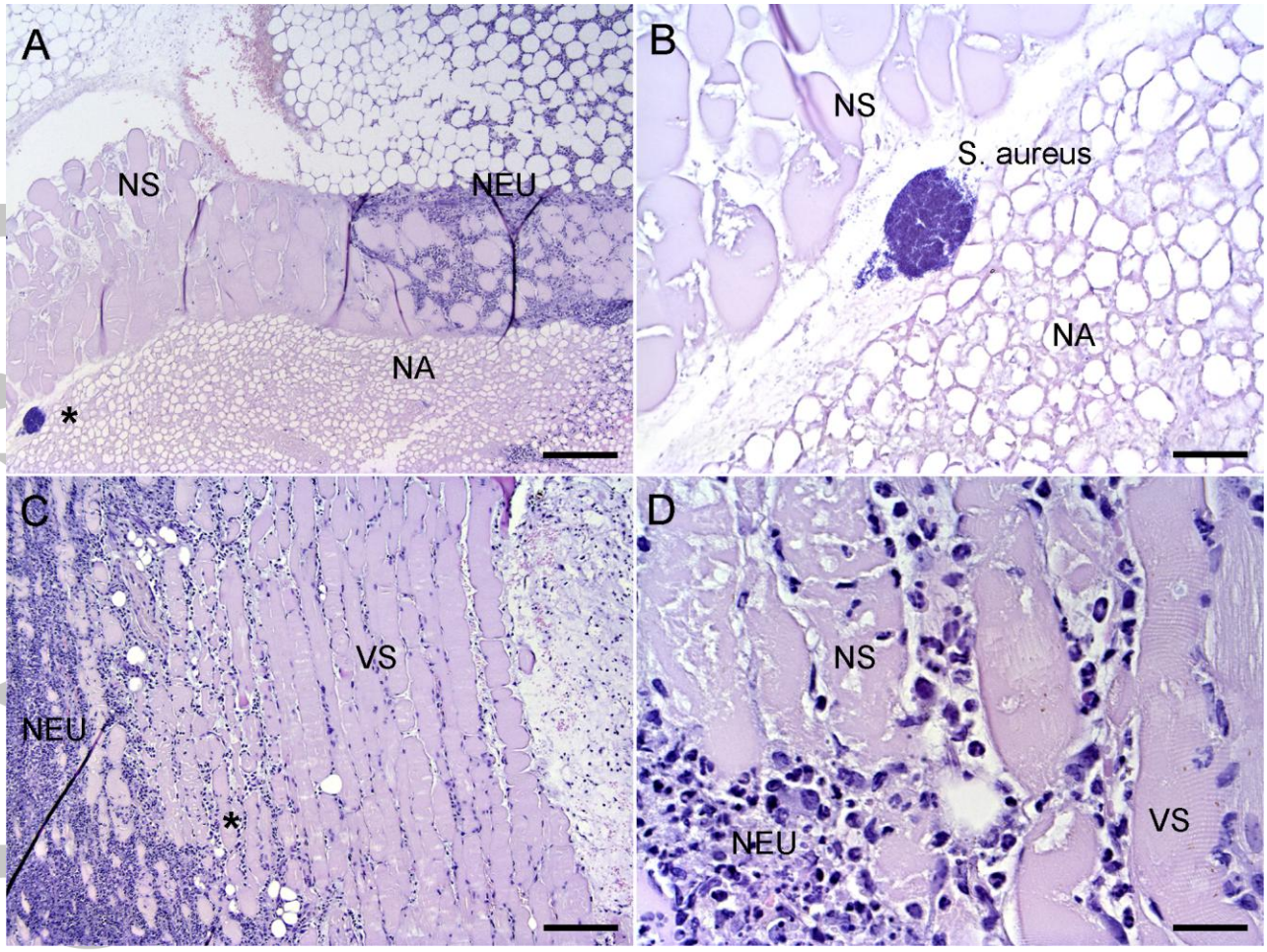

Figure 3: Histopathology of skin lesions in mice approximately 24 hours after inoculation with *S. aureus* (A and B) or injection with turpentine oil (C and D). Area in A and C marked with an asterisk (*) are enlarged and presented as B and D, respectively. Essentially the lesions, whether induced by *S. aureus* (A and B) or turpentine oil (C and D), are identical: striated muscle (NS) and adipose tissue (NA) presents with necrosis, and these areas are demarcated and infiltrated with neutrophils (NEU); viable striated muscle (VS) and viable adipose tissue is located peripheral to the necrotic centers. A bacterial colony (S. aureus) is present in the mouse inoculated with *S. aureus*. Haematoxylin and eosin staining. Bars: 160 µm (A and C), 40 µm (B), and 25 µm (D).

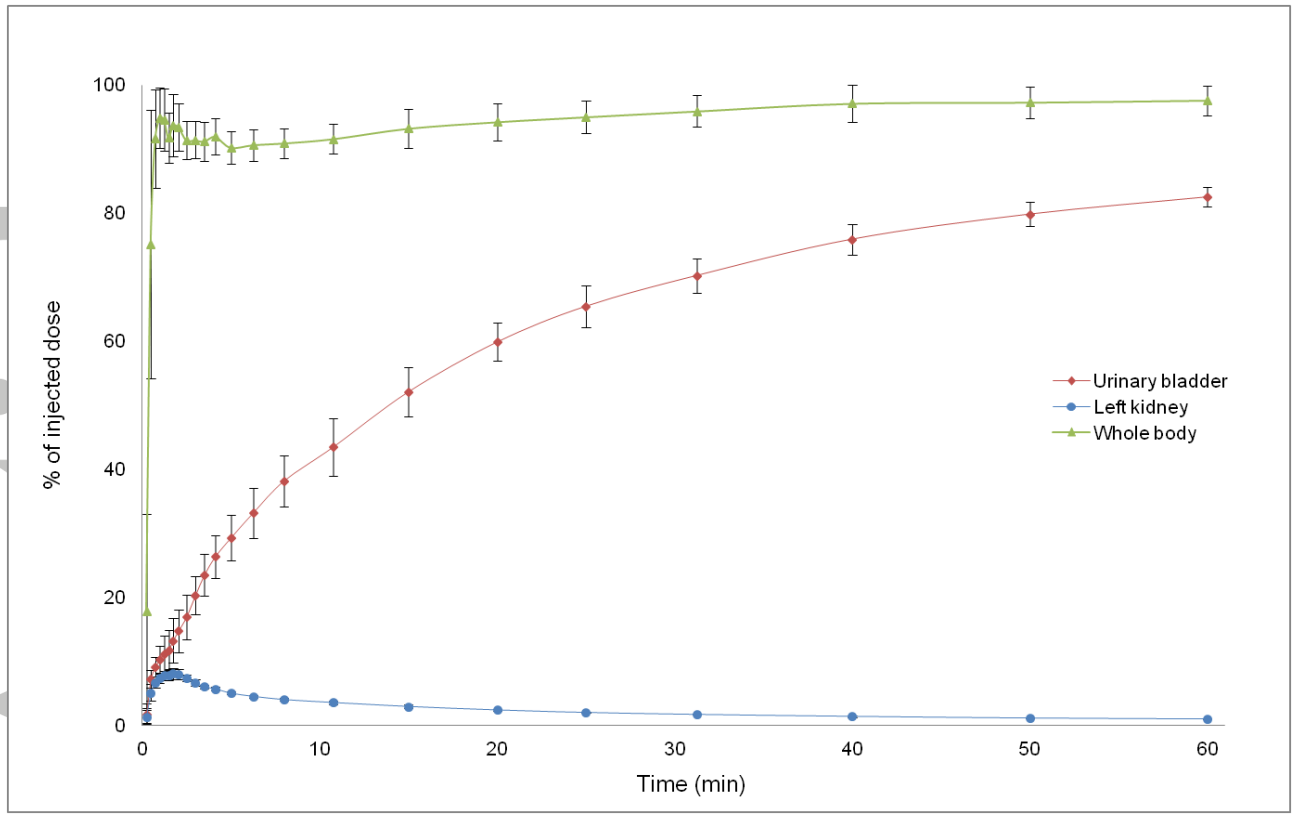

Figure 4: Distribution of radioactivity within the field of view during µPET scan of [^{68}Ga]DOTA-K-A9 as percentage of the injected dose. Results are given as mean ± SD and based on mice No. 6, 9, 12, and 15 with injected doses in the range of 3.7-10.4 MBq.

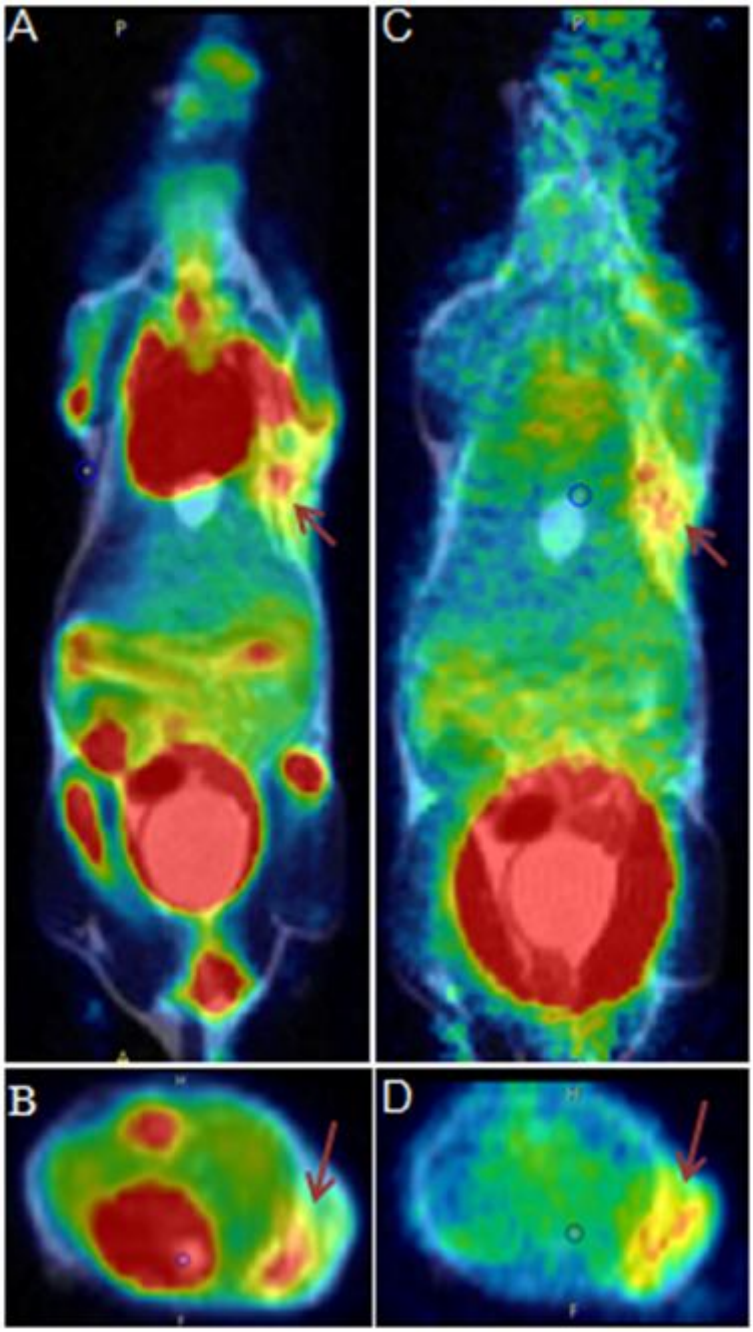

Figure 5: µPET/MRI scans of mouse No. 3 with subcutaneous *S. aureus* infection. Images of [^{18}F]FDG (8.9 MBq) in coronal plane dorsal view (A) and transversal plane caudal view (B). Images of [^{68}Ga]Ga-DOTA-K-A9 (3.8 MBq) in coronal plane dorsal view (C) and transversal plane caudal view (D). All images are summed from 60 - 90 min. The red arrows indicate the infectious focus with accumulation of both tracers. Additional, [^{68}Ga]Ga-DOTA-K-A9 showed a low background binding with most of the radioactivity being in the urinary bladder.

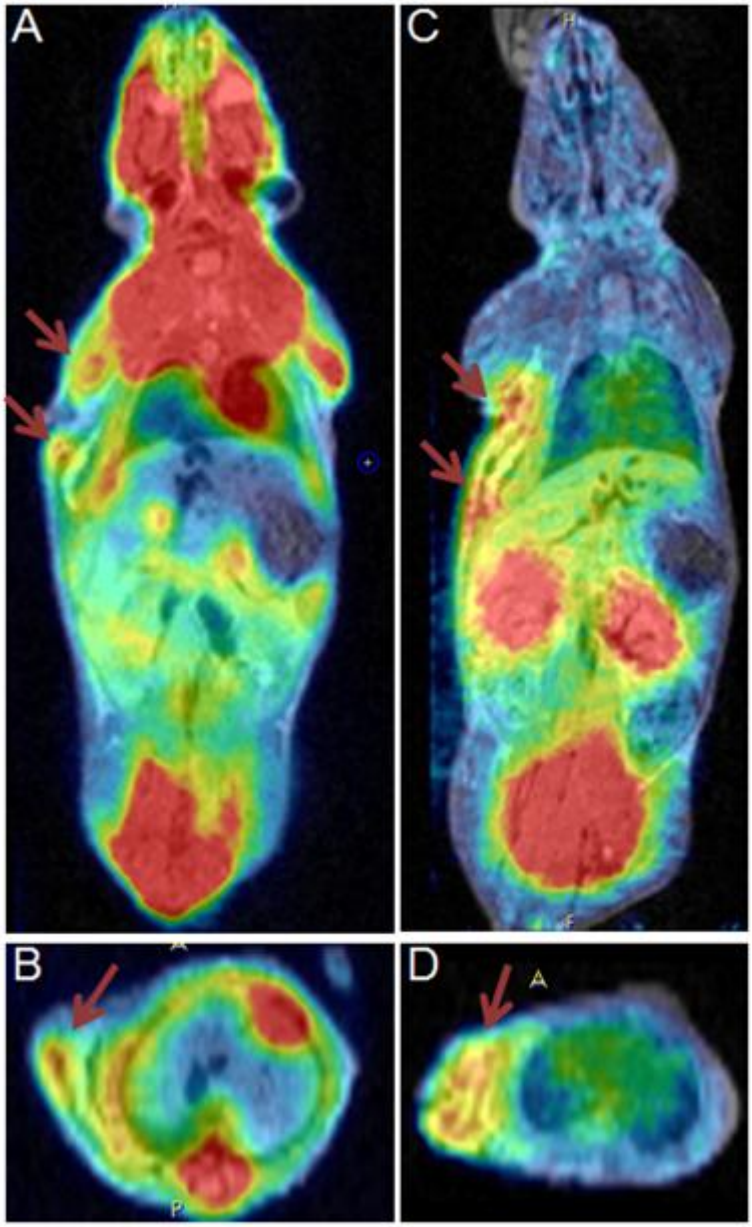

Figure 6: µPET/MRI scans of mouse No. 12 with subcutaneous *S. aureus* infection. Images of [^{18}F]FDG (9.7 MBq) in coronal plane ventral view (A) and transversal plane caudal view (B). Images of [^{68}Ga]Ga-DOTA-K-A9 (4.8 MBq) in coronal plane ventral view (C) and transversal plane caudal view (D). All images are summed from 30 - 60 min. The red arrows indicate the infectious focus exclusively with accumulation [^{68}Ga]Ga-DOTA-K-A9, while the yellow arrow illustrates [^{18}F]FDG accumulation in brown adipose tissue.

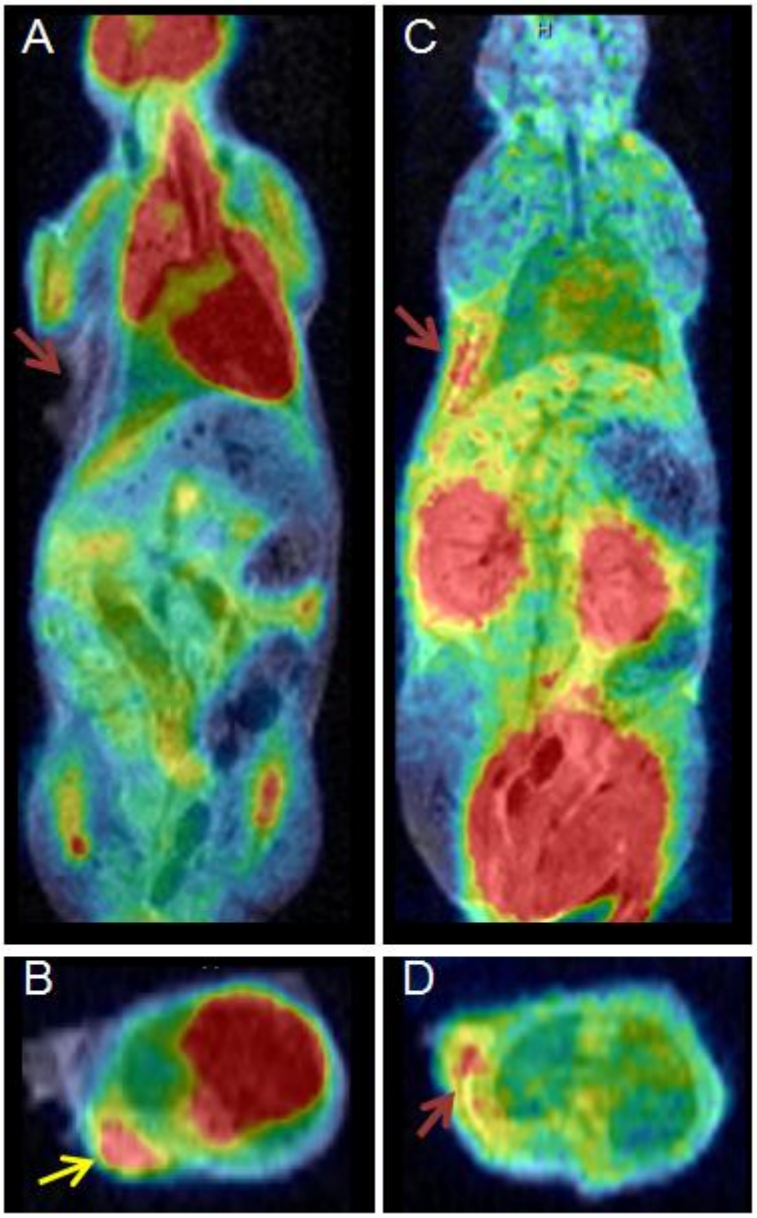

Figure 7: µPET/MRI scans of mouse No. 4 with subcutaneous turpentine induced inflammation. Images of [^{18}F]FDG (18.9 MBq) in coronal plane ventral view (A) and transversal plane caudal view (B). Images of [^{68}Ga]Ga-DOTA-K-A9 (11.5 MBq) in coronal plane ventral view (C) and transversal plane caudal view (D). All images are summed from 30 - 60 min. The red arrows indicate the inflammatory foci with a similar accumulation pattern of both tracers.

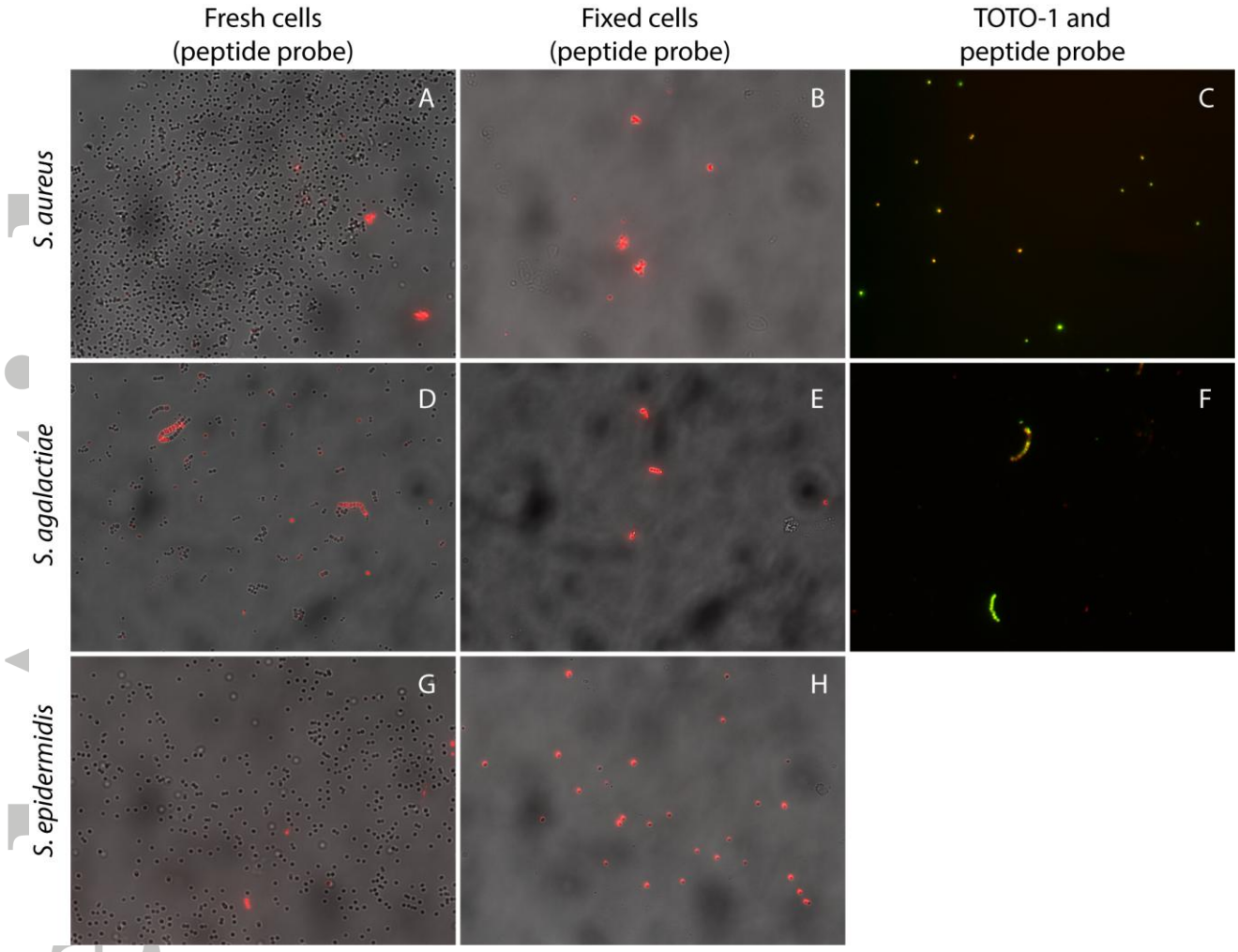

Figure 8: Epifluorescence imaging of TAMRA-K-A9 (red) binding to *S. aureus* (A-C), *S. agalactiae* (D-F) and *S. epidermidis* (G-H). The peptide probe only bound to few cells if the cells were prepared fresh (A+D+G), whereas all cells appeared to bind the probe if they had been killed and fixed (B+E+H). To verify if only cells with a damaged membrane would bind the peptide probe, we combined peptide labelling with the membrane-impermeable DNA stain TOTO®-1 (green) (C+F). Cells binding both TOTO®-1 and the peptide probe appear yellow-orange, and the images confirm that only cells with a damaged membrane would bind the peptide probe, which indicates an intracellular epitope.